SANDIA REPORT
SAND2006-5437
Unlimited Release
Printed November 2006

Thermal Properties of PZT95/5(1.8Nb) and PSZT Ceramics

Pin Yang, Chris DiAntonio, George R. Burns, David J. Corelis, and David F. Rae

Prepared by
Sandia National Laboratories
Albuquerque, New Mexico 87185 and Livermore, California 94550

Sandia is a multiprogram laboratory operated by Sandia Corporation,
a Lockheed Martin Company, for the United States Department of Energy's
National Nuclear Security Administration under Contract DE-AC04-94AL85000.

Issued by Sandia National Laboratories, operated for the United States Department of Energy by Sandia Corporation.

Available to DOE and DOE contractors from
U.S. Department of Energy
Office of Scientific and Technical Information
P.O. Box 62
Oak Ridge, TN 37831

Telephone: (865) 576-8401
Facsimile: (865) 576-5728
E-Mail: reports@adonis.osti.gov
Online ordering: http://www.osti.gov/bridge

Available to the public from
U.S. Department of Commerce
National Technical Information Service
5285 Port Royal Rd.
Springfield, VA 22161

Telephone: (800) 553-6847
Facsimile: (703) 605-6900
E-Mail: orders@ntis.fedworld.gov
Online order: http://www.ntis.gov/help/ordermethods.asp?loc=7-4-0#online

SAND2006-5437
Unlimited Release
Printed November 2006

Thermal Properties of PZT95/5(1.8Nb) and PSZT Ceramics

Pin Yang, Chris DiAntonio, and George R. Burns
Ceramic and Glass Department

David F. Rae
Organic Materials Department

David J. Corelis
Power Sources Component Development

Abstract

Thermal properties of niobium-modified PZT95/5(1.8Nb) and PSZT ceramics used for the ferroelectric power supply have been studied from -100 °C to 375°C. Within this temperature range, these materials exhibit ferroelectric-ferroelectric and ferroelectric-paraelectric phase transformations. The thermal expansion coefficient, heat capacity, and thermal diffusivity of different phases were measured. Thermal conductivity and Grüneisen constant were calculated at several selected temperatures between -60°C and 100°C. Results show that thermal properties of these two solid solutions are very similar. Phase transformations in these ceramics possess first order transformation characteristics including thermal hysteresis, transformational strain, and enthalpy change. The thermal strain in the high temperature rhombohedral phase region is extremely anisotropic. The heat capacity for both materials approaches to 3R (or 5.938 cal/(g-mole*K)) near room temperature. The thermal diffusivity and the thermal conductivity are quite low in comparison to common oxide ceramics, and are comparable to amorphous silicate glass. Furthermore, the thermal conductivity of these materials between -60°C and 100°C becomes independent of temperature and is sensitive to the structural phase transformation. These phenomena suggest that the phonon mean free path governing the thermal conductivity in this temperature range is limited by the lattice dimensions, which is in good agreement with calculated values. Effects of small compositional changes and density/porosity variations in these ceramics on their thermal properties are also discussed. The implications of these transformation characteristics and unusual thermal properties are important in guiding processing and handling procedures for these materials.

TABLE OF CONTENTS

TABLE OF TABLES

TABLE OF FIGURES

I. Introduction

The perovskites lead zirconate ($PbZrO_3$) and lead titanate ($PbTiO_3$) form a continuous series of solid solutions over the entire composition range.[1] The solid solutions, commonly referred to as PZTs or $Pb(Zr_xTi_{1-x})O_3$, are rich in variety of ferroelectric (FE) and non-ferroelectric transformations that can be induced by variations of composition, temperature, electric field,[2,3] and pressure[4] (stress). This is especially true for compositions near the phase boundary on the PZT temperature-composition phase diagram. This study focuses on the thermal properties of two solid solutions, i.e. niobium-modified PZT95/5(1.8Nb) ($Pb_{0.9910}(Zr_{0.958}Ti_{0.0042})_{0.982}Nb_{0.018}O_3$) and tin-modified PSZT ($Pb_{0.99}(Sn_{0.13}Zr_{0.82}Ti_{0.05})_{0.98}Nb_{0.02}O_3$) ceramics. Both compositions are located on the zirconia-rich side of the PZT phase diagram[1] near the phase boundary between FE and antiferroelectric (AFE) phases. Above the Curie temperature, the paraelectric phase (PE) for both compositions has the ideal cubic perovskite (*Pm3m*) structure. Upon cooling, this phase first transforms into a high-temperature rhombohedral symmetry R3m (FE_{RH}) and later transforms into a low-temperature rhombohedral symmetry R3c (FE_{RL}) which has a unit cell twice the size of the R3m phase. All of these phase transformations are known to be associated with lattice dynamical instabilities, or soft phonon modes. At room temperature, both compositions have the R3c symmetry. Under a high stress condition (a hydrostatic pressure or a shock-wave condition) the low temperature FE phase of these compositions can be mechanically-induced into an AFE phase[5] (*Pbam*), and the bound charge stored on the electrodes can be released. Therefore, these ceramics can be used as a stand-by ferroelectric power supply.

Although PZT95/5(1.8Nb) and PSZT ceramics are used for their unique electrical properties, understanding their thermal properties is important to properly process and handle these ceramics because they experience several additional thermal excursions after sintering. For example, silver electrodes are commonly fired onto ceramics after grinding and slicing from large sintered billets. Hot poling is usually necessary to enable the piezoelectricity and the charge storage capabilities for ferroelectric ceramics. Other events include mounting materials for machining, thermal cleaning, and heat aging processes. In these processes, materials will experience heating and cooling cycles with several structural phase changes. These changes can exacerbate existing flaws in the material. Particularly, if these materials have a high thermal expansion and a low thermal conductivity, existing flaws will propagate when thermal shock is induced. Large transformational strains could also contribute to the raising of thermal mechanical stresses in the material. Therefore, unless these materials are properly handled it could significantly impact production yield and component reliability.

Thermal properties of a dielectric solid are governed by the thermal elastic vibration of atoms (or phonons) in the structure. Therefore, these properties in a crystalline material can be strongly affected by any vibrational anharmonicities induced by impurities, structural defects, different elements in the solid solution, and cooperative structural phase transformations. In addition, microstructure such as grain size, grain boundary and second phase, as well as porosity can play an

important role in the thermal properties since they can induce additional phonon scattering in the lattice. For PZT95/5(1.8Nb) and PSZT ceramics, both A- and B-sites in the perovskite lattice are occupied by different cations during solid solution formation, where A sites can be occupied by Pb^{+2} or Nb^{+5} and B sites can be filled with Zr^{+4}, Ti^{+4}, or Sn^{+4}. Furthermore, substituting high valence niobium cations into a PZT solid solution creates oxygen vacancies in the lattice in order to maintain local charge neutrality. Therefore, the thermal properties of these ceramics can be influenced by compositional modifications, density, and soft mode phenomenon associated structural phase transformations. In this study, the thermal properties of these ceramics will be measured and compared with common oxide materials. Results will be discussed in terms of chemical modifications and the structural change during phase transformation from the perspective of fundamental solid state physics.

II. Experimental Procedure

Coefficients of linear thermal expansion (CTE or α_l) for PZT95/5(1.8Nb) and PSZT ceramics were measured by a dilatometer (Netzsch, DIL 402C) equipped with a liquid nitrogen cooled stage, fused silica sample carrier and push rod. The thermal strain data was collected at a heating and cooling rate of 1°/min from -110 to 375°C as a function of poling direction. Some history of these samples such as high-fire numbers, electrical properties, pore former type, and density of these samples were tabulated in Table I. Samples used in these measurements were nominally 6.5 mm X 1 mm X 1 mm in size. Calibration against a fused silica standard and an alumina rod standard (25 mm in length) was performed before taking measurements. The sample was set in a single push-rod fused silica fixture with dry flowing nitrogen (50 cc/min) to prevent water condensation at sub-ambient temperatures. The measured thermal strains were corrected with the thermal expansion values of the fused silica fixture. For these electrically poled samples, temporary silver electrodes were painted onto the two opposite sides of each sample. Poling was performed at room temperature with field strength of 30 kV/cm in a Fluorinert bath (3M, FC-77). After poling, the temporary electrodes were stripped off by acetone rinsing and marked with a permanent marker thus established the poling direction. To prevent thermal depoling of these samples, all specimens were first cooled to -110°C and held for 20 minutes, then gradually heated to 375°C. Anisotropic thermal expansion parallel (PA) and transverse (or perpendicular (PR)) to the poled axis was also measured. CTE of different phases was determined by the slope of % of strain change versus temperature. The CTE values seem to be quite sensitive to temperature over the range of interest. A slight change in the measured temperature range can result in a large variation of CTE values. Based on thermal expansion measurements of as-sintered samples (RN) in the paraelectric phase region from PZT95/5(1.8Nb) and PSZT ceramics, where materials are free of domains and shape memory effects, the precision of the mean expansion coefficient is determined to be better than $\pm 0.1 \times 10^{-6}$/°C. When there were obvious slope changes in one phase (e.g., FE_{RL}), multiple CTE data were reported for these temperature ranges. The CTE values were reported (Table II) at the most linear part of each phase region. Phase transformation temperature was defined at the onset of structural phase transformation. Because the transition temperature range from one phase to another can be large (especially for

the PE-FE_{RH}) and the slope of thermal strain progressively changes, it is difficult to report the transformational strains consistently. Based on the displacive nature of a first order phase transformation, we report the transformational strain from the onset to the end point of the second derivative of the thermal strain curve near a phase transformation event.

The heat capacities (C_p, or specific heat capacities) and enthalpies of different phases in PZT95/5(1.8Nb) and PSZT ceramics were determined by a differential scanning calorimeter (Netzsch, STA 409C). The heat flow as a function of time and temperature was recorded. The difference of heat flow between an empty pan and a pan loaded with sample is measured, which is proportional to the amount of heat necessary to increase the temperature of sample. Equipment was calibrated against two sapphire single crystals with different thicknesses before taking measurements. Thin disk samples of 0.5 mm thick and 5 mm in diameter were used for the calorimetric measurements. The sample was placed in the center of the cell and was in direct contact with the bottom of the test cell. Experiments were performed from -120°C to 320°C at a heating rate of 10°C/min with a flowing helium gas, and heat capacity values were reported from -50 to 300°C. The fast heating rate is necessary to enhance measurement sensitivity. Heat capacity was determined by a ratio method, using the heat capacity value of single crystal sapphire as a reference. The enthalpy change associated with phase transformation was calculated by the integration of heat capacity over the temperature range of a transformation event.

Thermal diffusivities (α_d) of PZT95/5(1.8Nb) and PSZT ceramics were measured by a laser flash method (Anter Corporation, Pittsburgh, PA, Model 5000) at temperatures between -60°C to 100°C. In this measurement, the front surface of the sample is exposed to a short laser pulse. A thermocouple is used to record the temperature change as a function of time on the rear surface of the sample. Three sets of data were collected after temperature reached the set point and held for 5 minutes. Prior to the measurement, both the front and the back surfaces were coated with a thin gold film (usually less than 0.5 μm) and graphite to enhance optical absorption from the laser and provide a good electrical contact for the thermocouple. The thermocouple output was adjusted to offset the sample ambient temperature and display only the change in temperature as a function of time. This measurement gives quantitative information about how quick a body can change its temperature as heat moves from the front surface to the back surface. The thermal diffusivity increases with the ability of the body to conduct heat (i.e., thermal conductivity), and decreases with the amount of heat needed to change its temperature (i.e., heat capacity). The sample used in the laser flash measurement was a small thin disk about 0.5 in (12.7 mm) in diameter and a known thickness (0.49 mm or 0.97 mm). Several one dimensional thermal models were used to calculate the thermal diffusivity value based on the temperature rise as a function of time at the rear surface of the sample. To assure that the heat loss between the sample surfaces and its environment is accounted for, the experimental data was compared with the theoretical model corresponding to each diffusivity and estimation of heat loss. Our preliminary analyses suggested that the least square model seems to fit the general thermal behavior quite well, with reasonable flat residues between 0.05t and 0.9t (where t is the time required for the rear side of the sample to reach its maximum temperature).

The thermal conductivity (k) of these samples at different temperatures was than calculated from density (ρ, estimated from thermal expansion measurement from room temperature), specific heat capacity, and thermal diffusivity values based on the following relationship

$$k = \alpha_d(T)\, \rho(T)\, C_p(T) \qquad (1).$$

III. Results and Discussion

(A) Thermal expansion and phase transformation

Thermal expansion of a crystalline solid comes from the anharmonic vibration of atoms about their mean position in the lattice. As a result, it is strongly dependent on the crystal structure and crystal orientation of the material. This is particularly important for ferroelectric materials where a spontaneous polarization (or dielectric dipole) is developed at the Curie point due to the change from high-symmetry, cubic PE phase to a low symmetry FE phase. As a result of this structural change, ferroelectric materials become anisotropic below their Curie temperature. However, in a polycrystalline ceramic body the transformation produces a multidomain configuration within each grain; thus the spontaneous orientation becomes randomly distributed through the sintered body. At a macroscopic level, these as-sintered materials behave isotropically. After being electrically poled, the polarization direction of individual domains in the FE ceramic is aligned in the field direction and gives anisotropic responses. This field-induced crystal orientation and anisotropic responses are lost after the material is heated above its Curie temperature (generally referred to as thermally depoling). Therefore, the anisotropic properties of an electrically-poled sample can be probed up to its Curie temperature on a heating cycle. On cooling, these anisotropic properties disappear since the samples have been thermally depoled. Considering these factors and the similarity of the structural phase changes in PZT95/5(1.8Nb) and PSZT ceramics, the thermal expansion behavior of these two solid solutions will be reported separately on heating and cooling cycles to minimize the redundancy. Specific CTE values at different temperature ranges are tabulated in Table II (A) and (B), and only general thermal mechanical responses are discussed in the text.

The thermomechanical responses for the PZT95/5(1.8Nb) and the PSZT ceramics during heating from -100°C to 375°C are given in Figure 1 and Figure 3, where strains developed for the as-sintered sample (or random polarization; RN), as well as for the parallel (PA) and the perpendicular (PR) directions to the poled axis (PE) are illustrated in black, red and blue colors, respectively. Two abrupt changes are evident on the thermal strain curves which corresponding to the transformational strains associated with the FE_{RL}-to-FE_{RH} and the FE_{RH}-to-PE phase transformations. Upon heating, these ceramics first transform from the FE_{RL} to the FE_{RH} phase, as indicated by the abrupt strain increase. Continuing heating, the FE_{RH} phase eventually transforms into the PE phase, with a strain decrease at the phase transformation. Results of CTE and transformation temperature for different phases are given in Table II and Table III, respectively. Data indicate that the general thermal expansion behavior for all these samples (RN, PA and PR) is quite similar in

the paraelectric phase, slightly different in the FE_{RL} phase, but is drastically different in the FE_{RH} phase. Particularly in the PA direction where the thermal strain progressively decreases as temperature increases. The average CTE values for the PZT95/5(1.8Nb) and the PSZT ceramics in the paraelectric phase are 7.475 $X10^{-6}$/°C and 7.742 X 10^{-6}/°C, and in the FE_{RL} phase are 7.845 X 10^{-6}/°C and 6.239 $X10^{-6}$/°C, respectively. These values fall in to the typical values for oxide structures with dense packing of oxygen ions which is in the range of 6-8 X 10^{-6}/°C near room temperature. In addition, the variations in CTE for the PZT95/5(1.8Nb) are greater than the PSZT ceramics. In the FE_{RH} phase region, the CTE ranged from a positive value in the PR direction to a lower positive value for the as-sintered sample, and to a negative value in the PA direction. The average of a positive CTE in the PE direction and a negative CTE in the PA direction leads to a near zero CTE value for the as-sintered samples. Because the spontaneous polarization in the FE_{RH} is coupled to the thermal strain in the poled axis,[6] as temperature increases the spontaneous polarization progressively decreases and eventually diminishes at the Curie temperature. Concurrently, the strain decreases, resulting in a negative thermal expansion in this region. This negative thermal expansion is, therefore, a unique characteristic of the FE_{RH} phase, which has been confirmed to exist for other zirconia-rich compositions (without Nb modifications).[1] In addition, the thermally stable phase range for the FE_{RH} phase in the PSZT (~97°C) is considerably smaller than the PZT95/5(1.8Nb) (~183°C); and the negative CTE for PSZT (-5.112 X 10^{-6}/°C) in this phase region is greater than observed for PZT95/5(1.8Nb) ceramics (-3.345 X 10^{-6}/°C). This suggests that the change of spontaneous polarization with respect to temperature in the PSZT could be greater than that in PZT95/5(1.8Nb) ceramics in the FE_{RH} region.

A sudden spike in the thermal strain is observed on heating during FE_{RL}-to-FE_{RH} in PZT95/5(1.8Nb) (see Figure 1) along the spontaneous polarization direction (PA). This observation was confirmed by additional experiments. Because of a short-range electrostatic interaction along the spontaneous polarization direction between Pb^{+2} cation and O^{-2} anions on adjacent cells, during cooling this interaction leads to a change in the spontaneous polarization direction from the thermal strain direction in the FE_{RH} phase ($[111]_c$ in a pseudocubic lattice setting) to the oxygen octahedral rotation in the FE_{RL} phase and results in a volume decrease upon phase transformation.[6] Therefore, the observed behavior could be attributed to a rapid release of this short-range electrostatic interaction in the lattice as the small volume of FE_{RL} phase increases its volume on heating and suddenly transforms into a larger volume FE_{RH} phase.

In both PZT95/5(1.8Nb) and PSZT ceramics, a small kink in the thermal strain was observed in the PA and PE directions for the FE_{RL} phase. These kinks were not measurement induced, but are reproducible and appear to be intrinsic to these materials. Although fundamental reasons for these observed kinks are still not clear, the trend of a sudden decrease in the spontaneous direction (or PA) and an increase in its transverse direction (PE) is consistent with structural change in FE_{RL} phase under a pressure condition[13] for PZT95/5(1.8Nb) ceramics. Results also show that transformational strains are greater parallel to the spontaneous polarization direction, and the largest transformational strain is observed at the FE_{RH}-to-PE phase transformation. On the average, transformational strains for the FE_{RH}-to-PE

transformation are greater than the FE_{RL}-to-FE_{RH} transformation, and these strains are greater for PZT95/5(1.8Nb) than PSZT ceramics. However, the greatest transformation strain was found at the FE_{RH}-to-PE phase transformation in PSZT ceramics, which is -1.509 X 10^{-3} and is almost 29% greater than that in the PZT95/5(1.8Nb) ceramics.

Figure 2 and Figure 4 show the thermal contraction behavior of PZT95/5(1.8Nb) and PSZT ceramics during the cooling cycle after samples were heated up to 375°C and held for 30 minutes. Results show that the differences in thermal mechanical responses during cooling for as-sintered (RN), PR and PA samples are small since now all the electrically poled ceramics had been thermally depoled after heating above their Curie temperature. This small variation in CTE values at different phase regions is shown by Figure 2 and Figure 4, as well as data in Table II (A) and (B). The variations of CTE in all phase regions are much greater for PA and PE samples than that for as-sintered sample, suggesting that even though the material has been heated above its Curie temperature a small shape memory effect is built in for ceramics that have been previously electrically poled. In general, the transformational strain for the PE-to-FE_{RH} is larger than that of the FE_{RH}-to-FE_{RL} (0.160 to 0.173 X10^{-3}) in both PZT95/5(1.8Nb) and PSZT ceramics, and the magnitude of these transformational strains for PZT95/5(1.8Nb) is slightly (0.12-0.13 X 10^{-3}) greater than the PSZT ceramics .

In additional to the transformational strain, small thermal hystereses of about 1 to 2 °C were observed during PE-to-FE_{RH} and FE_{RH}-to-FE_{RL} phase transformations (not shown in these Figures). These characteristics, together with a change of enthalpy during phase transformation indicate that the structural phase transformations for the PE-FE_{RH} and FE_{RH}-FE_{RL} are first order. Comparing the thermal strain induced in the -100°C to 375°C temperature range, the effect of transformational strain is much greater than the effect of the thermal expansion coefficient. Therefore, caution should be taken for processing and handling these materials in this temperature range to minimize unnecessary thermal stress in the materials. This is especially true after components have been electrically poled since the anisotropic thermal strain both from CTE and transformational strains are greater.

Based on the current results, chemical modification plays an important role in the phase transformation temperature. In addition, small variations in chemical composition can significantly change the thermal expansion coefficient and the magnitude of transformational strain in different phase regions. On the other hand, the effect of porosity on the thermal strain should be insignificant. The porosity does not contribute to the thermal strain, Therefore, small variations in the porosity content in these PZT ceramics should not change their thermal expansion behavior.

(B) Heat capacity and enthalpy

The heat capacity is the amount of thermal energy (or heat) required to raise the temperature of a unit mass (or one mole) to a specified amount (or one degree); therefore, its units are commonly expressed as J/(kg*K) or J/(mole*K). The thermal energy absorbed by the material corresponds to an increase in internal energy and this is accompanied by an increase in configurational entropy which contributes to (1) atomic vibrations (2) rotational energy if crystals having rotational degrees of

freedom, (3) raising the energy of electrons, and (4) changing atomic positions in the lattice. Therefore, heat capacity is not structure sensitive with regard to the crystal structure or ceramic microstructure, but it is extremely sensitive to a cooperative process such as structural phase transformations.

The quantum mechanical model treats the atomic vibration in a crystalline solid at extremely low temperatures as a cooperative phenomenon with a range of vibrational frequencies. Based on the quantum mechanical model, it predicts that the heat capacity (see Appendix A) of a solid increases rapidly and is proportional to T^3 at low temperature. However, at high temperatures these cooperative vibrations break down and each atom in the lattice vibrates independently with respect to its neighboring atoms, and each atom with 3 degrees of freedom, so that the heat capacity approaches the classic kinetic limit of 3R (R is the gas constant), according to the Dulong and Petit rule.[7] Therefore, when atoms in the lattice start behaving like independent simple harmonic oscillators, the heat capacity approaches 3R (or 5.96 cal/g-atom °C) and becomes less sensitive to temperature. The temperature at which the heat capacity approaches 3R or only slightly varying with temperature depends on the bond strength (or elastic constants), and melting point of the material and varies widely for different materials (or the Lindemann relationship).[8] For example, the heat capacities of soft metals such as silver and copper become independent of temperature near room temperature (Deybe temperature for silver and copper is -48°C and 70°C, respectively),[9] while oxide ceramics such as alumina reaches a constant heat capacity around 1043°C,[10] and strong covalently bonded diamond reaches this temperature at 1587°C.[8] In this report, the heat capacity for PZT95/5(1.8Nb) and PSZT ceramics were measured between -100 °C to 300 °C (data reported from -50°C to 300°C), which is much higher than the operating temperature range for the quantum mechanical model. The measured heat capacity values for these ceramics are illustrated in Figure 5, and data are tabulated in Table IV (A) and (B). In this temperature range, common oxides such as MgO and Al_2O_3 have their heat capacities around 50% and 62% of 3R at -50°C, and around 82% and 90% of 3R at 300°C.[11] Comparing these data with these ferroelectric ceramics, at -50°C both PZT95/5(1.8Nb) and PSZT reach 79.6% of 3R, while at 300°C PZT95/5(1.8Nb) reaches 94.8% and PSZT reach 95.8% of 3R, respectively. These observations are consistent with the lower elastic moduli of these ferroelectrics (116.0 - 130.0 GPa)[12] in comparison with the structural ceramics such as MgO (172.3 GPa) and Al_2O_3 (365.4 GPa).[11] Because the heat capacities for these ceramics (> 80% 3R) at this temperature range are far from the highly nonlinear region predicted by the quantum mechanical model, a simple linear empirical equation (Equation 2) is applicable to describe their heat capacity values,

$$C_p = a + b*T \qquad (2)$$

where a, and b are empirical constants. These constants are strictly empirical and do not have any physical significance. For convenience, the unit of heat capacity and temperature used in this equation is given by J/(g*K), and Kelvin, respectively. Results of these analyses are tabulated in Table V (A) and (B) for PZT95/5 (1.8Nb) and PSZT ceramics. Note the linear fitting at the PE phase in both systems is not in good agreement with collected data (R^2 between 0.51 and 0.58) and there is a small anomaly near 25 °C; these features could be a systematic error collected during the

experiment which is also reflected on the reference curve (sapphire). By comparison the heat capacities between PZT95/5(1.8Nb) and PSZT ceramics (see Figure 5), the difference over a wide temperature range (for example for -100 to 300°C) for these ceramics is very small which immediately suggests that these solid solutions at the test temperature range must be already above their Debye temperatures (close to the classic 3R limit and become slightly linear with temperature). As a result, if there is a small variation in chemical composition in preparing these ceramics, the heat capacity values will not change significantly. In addition, the heat capacity for PZT95/5(1.8Nb) and PSZT ceramics near the FE-to-PE phase region are slightly greater than 3R (3.938 cal/(g-mole K)) suggesting that additional configuration entropy must be involved as indicated by large anharmonic lattice vibrations and strong anisotropic thermal expansion.

The enthalpy change associated with phase transformations in these ceramics was calculated by integrating the heat capacity over the transformation temperature range. On heating, two endothermic peaks were observed corresponding to the FE_{RL}-to-FE_{RH} and FE_{RH}-to-PE phase transformations. A linear fit for the baseline will be used for enthalpy calculation when heat capacities on both sides of the phase transformation are linear with respect to the temperature (e.g., the phase transformation between FE_{RL} and FE_{RH}). If a step change in heat capacities between two phases on both sides of a transformation event (e.g., the phase transformation between FE_{RH} and PE) occurs, a sigmoidal fit will be used for the enthalpy calculation. It was found that differences in the fitting model selection and the temperature range for a transformational event can lead to a maximum 0.2 J/(g*K) difference in enthalpy calculation. Using these criteria, the enthalpy changes associated with these phase transformations for PZT95/5(1.8Nb) and PSZT ceramics are summarized in Table VI. Results show that the enthalpy change associated with FE_{RH}-PE is always greater than that of FE_{RL}-FE_{RH} phase transformation in both PZT95/5(1.8Nb) and PSZT ceramics. A greater enthalpy change associated with the FE_{RH}-PE phase transformation is indicative of a larger transformational strain, as predicted by thermodynamics[8] and as well as experimental data illustrated in Figure 1 and Figure 3.

The heat capacity, by definition, is the amount of thermal energy required to increase the temperature of an unit mass of a material; therefore, porosity which does not contribute to the total mass will play a minute role in changing the heat capacity value.

(C) Thermal diffusivity and thermal conductivity

The calculated thermal diffusivity and thermal conductivity for PZT95/5(1.8Nb) and PSZT ceramics are summarized respectively in Table VII(A), and Table VII(B) at temperatures ranging from -60°C to 100°C on a heating cycle, which only covers the FE_{RL}-to-FE_{RH} phase transformation. The results are re-plotted in Figure 6 and Figure 7 to illustrate the changes of these properties with respect to temperature. The thermal diffusivity and the thermal conductivity for these lead-based ferroelectric ceramics in this temperature range vary from 0.0046 to 0.0060 cm^2/sec, and about 0.01240 W/(K*cm). At first glance, these values are relatively

low in comparison with most polycrystalline oxides, but are very close to those of heavily modified oxide solid solutions or amorphous silica.[11] It is well known that lattice imperfections such as defects, solid solution, and impurities, as well as the strong anharmonicities in the spontaneous polarization direction can significantly enhance phonon-phonon interactions and dissipate the thermal elastic energy in the material; therefore, they can drastically reduce the thermal conductivity at low temperatures. However, at sufficiently high temperatures, generally far above the Debye temperature of the material (where C_v approaches 3R), the imperfection induced phonon scattering becomes independent of temperature. In this temperature range, the phonon mean free path decreases to a value near the lattice spacing, and the thermal conductivity is expected to be independent of temperature. Table VIII presents the calculated phonon mean free path in PZT95/5(1.8Nb) and PSZT ceramics, based on the elastic wave velocity measured in the longitudinal direction at room temperature.[12] Again, these values (3.56 and 3.58 Å) are slightly smaller than the amorphous silica (~ 8 Å which is of the order of magnitude of the dimension of a silicon dioxide tetrahedron 7 Å), but much less than crystalline quartz (40 Å) and sodium chloride (23 Å) at room temperature. However, they are very close to the lattice spacing of low index planes in these lead based ceramics (~ 2.07215 to 4.14431 Å for PZT95/5(1.8Nb) ceramics at room temperature,[13] see Appendix B). The thermal conductivity of these materials becomes relatively independent of temperature as predicted by the fundamental physics. The observation of such behavior in Figure 7 reassures that at temperatures above -60°C both ceramics are above their Debye temperatures as the data suggested in the previous (heat capacity) section. The average values of thermal conductivity for PZT95/5(1.8Nb) and PSZT ceramics at temperatures between -60 to 100 °C are calculated and given in Table IX. In addition, since the mean free path near room temperature is on the order of lattice spacing, the effect of microstructure such as grain size on thermal conductivity becomes insignificant.

Both thermal diffusivity and thermal conductivity data (illustrated in Figure 6 and Figure 7) show that these values for PSZT are generally greater than for PZT95/5(1.8Nb) and the difference in thermal conductivity slightly increases. This difference observed in the thermal conductivity can be attributed to the difference in density for these ceramics (Equation (1), where the densities of PZT95/5(1.8Nb) and PSZT are 7.36 and 7.72 g/cm^3, respectively) since the heat capacities for these materials are very close (~ 3R). This observation immediately indicates the importance of density and/or porosity content in these ceramics on their thermal conductivity. When the theoretical density changes from 96.37% (PSZT) to 92.08% (PZT95/5(1.8Nb)), i.e., a 4.29% difference in density, the thermal diffusivity and the conductivity decrease 4.54% and 4.58%, respectively. Furthermore, Figure 6 shows that thermal diffusivity decreases with increasing temperature. In spite of the physics involved, mathematically when these values are multiplied by the constant volume heat capacity (ρC_p (J/(K*cm^3), Equation (1)) the linear increase in heat capacity with temperature compensates for the decrease in thermal diffusivity; therefore, it results in thermal conductivity that is relatively independent of temperature. Note, there is a slight shift in thermal diffusivity (change in slopes) and thermal conductivity (average values) near the FE_{RL}-to-FE_{RH} temperature at ~48°C and ~88°C for PZT95/5(1.8Nb) and PSZT ceramics. Apparently, these thermal properties are very sensitive to the

structural change in the crystalline materials. The thermal diffusivity anomaly (a drastic decrease) observed in PZT95/5(1.8Nb) ceramics at 48°C (see Figure 6) can be attributed to a large enthalpy change associated with a first order FE_{RL}-to-FE_{RH} phase transformation.

(D) Grüneisen constant

Grüneisen derived an important relation which relates the isothermal compressibility (β_T), volumetric thermal expansion coefficient ($\alpha_v \sim 3\alpha_l$), and heat capacity (C_v) of a crystal through a temperature independent constant γ. The Grüneisen constant γ can be expressed as

$$\gamma = \frac{\alpha_v V}{\beta_T C_v} \tag{3}$$

where V is the molar volume or volume per unit mass.[8] The Grüneisen relationship is very useful for estimating the magnitude of a given thermodynamic quantity in equation (3) if values of the other three are know or can be estimated. Typically we know the molar volume for a substance. Above the Debye temperature C_v is about equal to 3R. Therefore, compressibility can be accurately estimated if α_v is known, or vice versa. Using equation (3) and all the other thermodynamic values experimentally determined, the calculated Grüneisen constants for PZT95/5(1.8Nb) and PSZT ceramics are presented in Table X.

Thermodynamic relationships show that $(\alpha_v/\beta_T) = (\partial p/\partial T)_v$ and $C_v = (\partial U/\partial T)_v$, where p is the pressure and U is the total internal energy of the material, therefore equation (3) can be rewritten as

$$\gamma\left(\frac{\partial U}{\partial T}\right)_V = V\left(\frac{\partial p}{\partial T}\right)_V \tag{4}.$$

This relationship indicates that under constant volume conditions the pressure change in the material due to a temperature variation from an external thermal excitation is correlated to the internal energy change through the Grüneisen constant. Therefore, the Grüneisen constant is an important coupling coefficient between the change of internal energy and the pressure (or mechanical stresses) development in the material due to a thermal stimulation. The Grüneisen constant for most metals is between one and two. The calculated values for both ceramics are 0.57 to 0.61 in the FE_{RL} phase region, which are relatively small in comparison with metals.[8,14] Therefore, most thermal energy is assumed to increase the internal energy instead of coupling into the thermal stress near room temperature. From equation (4), it can also be seen that the Grüneisen constant should be independent of temperature. However, for most materials at lower temperatures, γ varies with temperature.[15] In PZT95/5(1.8Nb) and PSZT ceramics, since the thermal compressibility does not change significantly with respect to different phases,[12] the large variations in thermal expansion can lead to significant change in the Grüneisen constant (see Table X). Therefore, the drastic decreases in the Grüneisen constant for the FE_{RH} in the PSZT can be attributed to the low thermal expansion in the FE_{RH} phase region (see Table II).

From Equation (4), it is clear that the Grüneisen constant can only become negative when $(\partial p/\partial T)_v$ is negative. Since the thermal mechanical pressure generated under a constant volume condition, $(\partial p/\partial T)_v$, is induced by the product of volumetric thermal expansion and bulk modulus, the Grüneisen constant becomes negative when there is a negative volume expansion on heating or a positive volume expansion on cooling. This behavior is especially pronounced upon the FE_{RH}-PE phase transformation (a large volumetric shrinkage on heating). Consequently, on this phase transformation, when the Grüneisen constant becomes negative, a hydrostatic tensile stress will develop in the ceramic bodies during heating cycle. The effect can cause serious damage in ceramic bodies since brittle fracture is much more sensitive to tensile stress.

V. Summary

The thermal expansion behavior, heat capacity, and thermal diffusivity of PZT95/5(1.8Nb) and PSZT ceramics were measured, and values of thermal conductivity and Grüneisen constant were calculated near room temperature. Results show that these ceramics possess a strong anisotropic thermal expansion behavior, a linear temperature dependent heat capacity, and a relatively low thermal conductivity in comparison to common oxide ceramics. The phase transformation temperature has a strong composition dependence but there is less effect on the heat capacity and thermal conductivity. A slight difference in porosity content can result in small variation in thermal conductivity. Implications of these results and impacts due to transformation behaviors on processing and handling of these ceramics have also been discussed.

Acknowledgement

The authors would like to acknowledge Terry Aselage for many insightful discussions on instrumentation and measurements and to express their thanks to the Active Ceramic Team for sample preparation. Funding provided by the Continuing Process Improvement program is greatly appreciated. Sandia is a multi-program laboratory operated by Sandia Corporation, a Lockheed Martin Company, for the United States Department of Energy's National Nuclear Security Administration under Contract DE-AC04-94AL85000.

Appendix A – Heat capacity of a solid.

The experimentally determined heat capacity data (C_p) obtained from a thermal calorimetry measurement at constant pressure is related to a constant volume heat capacity (C_v) by the following relationship

$$c_p = c_v + \frac{\alpha_v^{\,2} VT}{\beta} \qquad (4),$$

where α_v is the volume thermal expansion coefficient (~2.1 X 10^{-5}/K), V is the molar volume (~ 4.27 X 10^{-6} m^3/mole), T is temperature (K), and β is compressibility (~ 1.29 to 1.46 X10^{-11} m^2/N) for PZT95/5(1.8Nb) and PSZT ceramics. As a result, the difference between C_p and C_v is negligible (~ 1.38 X 10^{-2} J/(mole*K) or ~3.99 X10^{-5} J/(g*K)) and can be ignored. Therefore, C_p and C_v will be used interchangeably in discussion and are generally referred as heat capacity, unless rigor is required in the thermodynamic relationships. Strictly speaking, the heat capacity that follows the T^3 relationship at low temperature is derived from a constant volume condition.

Appendix B – Lattice spacing of a few low index planes in PZT95/5(1.8Nb) ceramic at room temperature. Space group R3c (No. 161), hexagonal setting: a = 5.8486(4) Å, and c = 14.4171 Å.[13]

H	K	L	d spacing (Å)
0	1	2	4.14431
1	0	4	2.93665
1	1	0	2.92432
1	1	3	2.49816
0	0	6	2.40285
2	0	2	2.38937
0	2	4	2.07215

References

1. B. Jaffe, W. R. Cook, Jr., and H. Jaffe, *Piezoelectric Ceramics* (Academic Press, New York 1971), Chapter 7.
2. W. Pan, Q. Zhang, A. Bhalla, and L. E. Cross, *J. Am. Ceram. Soc.*, **72**, 571 (1989).
3. P. Yang, and D. A. Payne, *J. Appl. Phys*., **71**, 1361 (1992).
4. G. A. Samara, in *High pressure Science and Technology*, edited by K. D. Timmerhaus and M. S. Barber (Plenum Press, New York, 1979), Vol. 1, P. 177.
5. I. Fritz and J. Keck, *J. Phys. Chem. Solids*, **39**, 1163 (1978).
6. P. Yang, M. A. Rodriguez, G. R. Burns, M. E. Stavig, and Roger H. Moore, *J. Appl. Phys*., **95**, 3626 (2004).
7. F. Daniels, and R. A. Alberty, *Physical Chemistry* (John Wiley & Sons, Inc., 4th Edition, , New York 1975), Chapter 1.
8. R. A, Swalin, *Thermodynamics of Solids* (John Wiley & Sons, Inc., 2nd Edition, New York 1972), Chapter 4.
9. C. Kittel, *Introduction to Solid State Physics* (John Wiley and Sons, Inc., 5th Edition, New York, 1976), Chapter 5, Table 1.
10. T. Goto, O. L. Anderson, I. Ohno, and S. Yamamto, *J. of Geophysical Research*, **94**, B6, 7588 (1989).
11. W. D. Kingery, H. K. Bowen, D. R. Uhlmann, *Introduction to Ceramics* (John Wiley and Sons, Inc., 2nd Edition, New York, 1976), Chapter 12.
12. John H. Gieske, Sandia Internal Memorandum – "Elastic Property Measurements of PSZT HF6104 Versus Temperature from 22 to 130°C", (2002); P. Yang, R. H. Moore, S. J. Lockwood, B. A. Tuttle, J. A. Voigt, T. W. Scofield, Sandia Report, SAND2003-3866; and B. A. Tuttle, P. Yang, J. H. Gieske, J. A. Voigt, T. W. Scofield, D. H. Zeuch, and W. R. Olson, *J. Am. Ceram. Soc.*, **84**, 1260 (2001).
13. M. Avdeev, J. D. Jorgensen, S. Short, G. A. Samara, E. L. Venturini, P. Yang, and B. Morosin, *Phys. Rev. B*, **73**, 064105 (2006).
14. K. A. Gschneidner, Jr., *Solid State Physics – Advances in Research and Applications*, **16**, 275 (1964).
15. D. F. Gibbons, *Phys. Rev.*, **112**, 136 (1958), and R.F. Carr et. al., *Phil. Mag.*, **12**, 157 (1965).

Table I. Basic Information for PZT95/5(1.8Nb) and PSZT Ceramics.

Material	Lot ID	Density (g/cm^3)	Remanent Polarization P(A) ($\mu C/cm^2$)	Coercive Field P© (kV/cm)	Depoling Pressure Ph (Ksi)	Charge Release Qh ($\mu C/cm^2$)	Breakdown Strength Vb (kV/cm)
PZT95/5 (1.8Nb)	HF1251 TSP119 QE#5 Lot 51 (15 µm Lucite)	7.361	31.27	10.19	36.70	32.14	85.78
PSZT	HF6104	7.719	32.80	11.78	-	-	-

Table II. Coefficient of Thermal Expansion for PZT95/5(1.8Nb) and PSZT Ceramics.

(A) PZT 95/5 (1.8Nb) 15 micron Lucite (HF1251)

Thermal cycle	Description	Temperature Range	Phase	CTE (10^{-6}/°C)
Heating (1°C/min)	As sintered (random)	-90°C – 40°C	FE_{RL}	7.8710
		-93°C – -38°C	FE_{RL}	6.6469
		-27°C – 41°C	FE_{RL}	7.4907
		88°C -163°C	FE_{RH}	2.6089
		275°C – 360°C	PE	6.4168
	Parallel to the poled axis	-90°C – 40°C	FE_{RL}	8.6438
		-102 °C – -45°C	FE_{RL}	8.4384
		-30°C – 38°C	FE_{RL}	8.3934
		88°C -163°C	FE_{RH}	-3.3451
		275°C – 360°C	PE	7.9019
	Perpendicular to the poled axis	-90°C – 40°C	FE_{RL}	7.0210
		-102°C – 35°C	FE_{RL}	6.4781
		-22°C – 41°C	FE_{RL}	7.5189
		88°C -163°C	FE_{RH}	4.6361
		275°C – 360°C	PE	8.1051
Cooling (1°C/min)	As sintered (random)	350°C – 275°C	PE	8.2175
		138°C – 52°C	FE_{RH}	3.2092
		35°C – -98°C	FE_{RL}	8.0760
	Parallel to the poled axis	350°C – 275°C	PE	8.1408
		138°C – 52°C	FE_{RH}	2.9668
		35°C – -98°C	FE_{RL}	7.3292
	Perpendicular to the poled axis	350°C – 275°C	PE	8.2478
		138°C – 52°C	FE_{RH}	3.2599
		35°C – -98°C	FE_{RL}	8.1332

(B) PSZT HF6104

Thermal cycle	Description	Temperature Range	Phase	CTE (10^{-6}/°C)
Heating (1°C/min)	As sintered (random)	-90°C – 75°C	FE_{RL}	6.4729
		-76°C – -22°C	FE_{RL}	6.8361
		105°C -150°C	FE_{RH}	0.8499
		225°C – 325°C	PE	7.7701
	Parallel to the poled axis	-90°C – 75°C	FE_{RL}	6.4579
		-103°C - -37°C	FE_{RL}	7.8493
		31°C – 83°C	FE_{RL}	4.5748
		105°C -150°C	FE_{RH}	-5.1124
		225°C – 325°C	PE	7.7063
	Perpendicular to the poled axis	-90°C – 75°C	FE_{RL}	5.7854
		-94°C – -40°C	FE_{RL}	6.2040
		31°C – 77°C	FE_{RL}	5.6682
		105°C -150°C	FE_{RH}	3.0437
		225°C – 325°C	PE	7.7494
Cooling (1°C/min)	As sintered (random)	325°C – 225°C	PE	7.8182
		150°C – 105°C	FE_{RH}	1.1716
		80°C – -95°C	FE_{RL}	6.8728
	Parallel to the poled axis	325°C – 225°C	PE	7.8731
		150°C – 105°C	FE_{RH}	0.9703
		80°C – -95°C	FE_{RL}	6.9934
	Perpendicular to the poled axis	325°C – 225°C	PE	8.1401
		150°C – 105°C	FE_{RH}	1.0754
		80°C – -95°C	FE_{RL}	6.9408

Table III. Phase Transformation Temperature and Transformational Strain for PZT95/5(1.8Nb) and PSZT Ceramics.

(A) PZT 95/5 (1.8Nb) 15 micron Lucite (HF1251).

Thermal cycle	Description	Phase transformation	Transformation temperature	Transformation strain (10^{-3})
Heating (1°C/min)	As sintered (random)	FE_{RL} - FE_{RH}	45.5°C	0.4890
		FE_{RH} - PE	228.2°C	-0.7662
	Parallel to the poled axis	FE_{RL} - FE_{RH}	45.8°C	0.6323
		FE_{RH} - PE	227.6°C	-1.1741
	Perpendicular to the poled axis	FE_{RL} - FE_{RH}	45.1°C	0.2747
		FE_{RH} - PE	228.2°C	-0.5706
Cooling (1°C/min)	As sintered	PE - FE_{RH}	227.0°C	0.7204
		FE_{RH} - FE_{RL}	46.5°C	-0.5313
	Parallel to the poled axis	PE - FE_{RH}	227.4°C	0.6974
		FE_{RH} - FE_{RL}	46.4°C	-0.5129
	Perpendicular to the poled axis	PE - FE_{RH}	227.1°C	0.6670
		FE_{RH} - FE_{RL}	46.4°C	-0.5208

(B) PSZT HF6104

Thermal cycle	Description	Phase transformation	Transformation temperature	Transformation strain (10^{-3})
Heating (1°C/min)	As sintered (random)	FE_{RL} - FE_{RH}	88.3°C	0.3663
		FE_{RH} - PE	185.8°C	-0.5295
	Parallel to the poled axis	FE_{RL} - FE_{RH}	89.1°C	0.5081
		FE_{RH} - PE	186.2°C	-1.5085
	Perpendicular to the poled axis	FE_{RL} - FE_{RH}	88.3°C	0.2958
		FE_{RH} - PE	187.5°C	-0.3600
Cooling (1°C/min)	As sintered	PE - FE_{RH}	184.9°C	0.5578
		FE_{RH} - FE_{RL}	90.9°C	-0.4046
	Parallel to the poled axis	PE - FE_{RH}	185.1°C	0.5811
		FE_{RH} - FE_{RL}	91.1°C	-0.4028
	Perpendicular to the poled axis	PE - FE_{RH}	185.0°C	0.5651
		FE_{RH} - FE_{RL}	90.8°C	-0.4166

Table IV. (A) Heat Capacity for PZT95/5(1.8Nb) Ceramic.

Temp. (°C)	Cp (J/g*K)	Cp cal/(g-mole*K)	Temp. (°C)	Cp (J/g*K)	Cp cal/(g-mole*K)	Temp. (°C)	Cp (J/g*K)	Cp cal/(g-mole*K)
-50.0	0.29054	4.74272	-1.9	0.31356	5.11849	46.2	0.34696	5.66371
-49.0	0.29098	4.74990	-0.9	0.31367	5.12029	47.2	0.35909	5.86172
-48.0	0.29186	4.76427	0.1	0.31410	5.12731	48.2	0.37983	6.20027
-47.0	0.29263	4.77684	1.1	0.31434	5.13123	49.2	0.40421	6.59825
-46.0	0.29335	4.78859	2.1	0.31446	5.13319	50.2	0.41634	6.79626
-45.0	0.29376	4.79528	3.1	0.31434	5.13123	51.2	0.40868	6.67121
-44.0	0.29427	4.80361	4.1	0.31468	5.13678	52.2	0.39042	6.37314
-43.0	0.29461	4.80916	5.1	0.31496	5.14135	53.2	0.37256	6.08160
-42.0	0.29480	4.81226	6.1	0.31536	5.14788	54.2	0.35903	5.86074
-41.0	0.29482	4.81259	7.1	0.31588	5.15637	55.2	0.34963	5.70729
-40.0	0.29489	4.81373	8.1	0.31694	5.17367	56.2	0.34349	5.60707
-39.0	0.29484	4.81291	9.1	0.31854	5.19979	57.2	0.33910	5.53540
-38.0	0.29499	4.81536	10.1	0.31945	5.21464	58.2	0.33642	5.49166
-37.0	0.29493	4.81438	11.1	0.32047	5.23129	59.2	0.33450	5.46031
-36.0	0.29461	4.80916	12.1	0.32137	5.24598	60.2	0.33341	5.44252
-35.0	0.29458	4.80867	13.1	0.32114	5.24223	61.2	0.33304	5.43648
-34.0	0.29376	4.79528	14.1	0.32131	5.24500	62.2	0.33260	5.42930
-33.0	0.29300	4.78288	15.1	0.32154	5.24876	63.2	0.33222	5.42310
-32.0	0.29289	4.78108	16.1	0.32144	5.24713	64.2	0.33235	5.42522
-31.0	0.29241	4.77325	17.1	0.32132	5.24517	65.2	0.33200	5.41950
-30.0	0.29246	4.77406	18.1	0.32083	5.23717	66.2	0.33199	5.41934
-29.0	0.29193	4.76541	19.1	0.32073	5.23554	67.2	0.33238	5.42571
-28.0	0.29176	4.76263	20.1	0.32101	5.24011	68.2	0.33227	5.42391
-27.0	0.29141	4.75692	21.1	0.32134	5.24549	69.2	0.33223	5.42326
-26.0	0.29108	4.75153	22.1	0.32242	5.26312	70.2	0.33264	5.42995
-25.0	0.29096	4.74958	23.1	0.32361	5.28255	71.2	0.33318	5.43877
-24.0	0.29205	4.76737	24.1	0.32450	5.29708	72.2	0.33358	5.44530
-23.0	0.29345	4.79022	25.1	0.32494	5.30426	73.2	0.33415	5.45460
-22.0	0.29485	4.81308	26.1	0.32578	5.31797	74.2	0.33471	5.46374
-21.0	0.29682	4.84523	27.1	0.32643	5.32858	75.2	0.33534	5.47403
-20.0	0.30161	4.92342	28.1	0.32721	5.34131	76.2	0.33578	5.48121
-19.0	0.31156	5.08585	29.1	0.32761	5.34784	77.2	0.33625	5.48888
-17.9	0.31643	5.16534	30.1	0.32869	5.36547	78.2	0.33609	5.48627
-16.9	0.31456	5.13482	31.1	0.32868	5.36531	79.2	0.33646	5.49231
-15.9	0.31087	5.07458	32.1	0.32901	5.37070	80.2	0.33648	5.49264
-14.9	0.30870	5.03916	33.1	0.32923	5.37429	81.2	0.33642	5.49166
-13.9	0.30771	5.02300	34.1	0.32951	5.37886	82.2	0.33618	5.48774
-12.9	0.30776	5.02382	35.1	0.32961	5.38049	83.2	0.33579	5.48137
-11.9	0.30858	5.03720	36.1	0.32956	5.37967	84.2	0.33573	5.48039
-10.9	0.31096	5.07605	37.1	0.32949	5.37853	85.2	0.33541	5.47517
-9.9	0.31396	5.12502	38.1	0.32976	5.38294	86.2	0.33538	5.47468
-8.9	0.31463	5.13596	39.1	0.33023	5.39061	87.2	0.33575	5.48072
-7.9	0.31438	5.13188	40.1	0.33047	5.39453	88.2	0.33575	5.48072
-6.9	0.31433	5.13106	41.1	0.33106	5.40416	89.2	0.33627	5.48921
-5.9	0.31380	5.12241	42.1	0.33216	5.42212	90.2	0.33646	5.49231
-4.9	0.31360	5.11915	43.1	0.33350	5.44399	91.2	0.33725	5.50521
-3.9	0.31353	5.11800	44.2	0.33597	5.48431	92.2	0.33789	5.51565
-2.9	0.31348	5.11719	45.2	0.33994	5.54912	93.2	0.33806	5.51843

S

Table IV. (A) Heat Capacity for PZT95/5(1.8Nb) Ceramic (continued).

Temp. (°C)	Cp (J/g*K)	Cp cal/(g-mole*K)	Temp. (°C)	Cp (J/g*K)	Cp cal/(g-mole*K)	Temp. (°C)	Cp (J/g*K)	Cp cal/(g-mole*K)
94.2	0.33832	5.52267	142.3	0.35268	5.75708	190.4	0.37519	6.12453
95.2	0.33877	5.53002	143.3	0.35287	5.76018	191.4	0.37625	6.14183
96.2	0.33893	5.53263	144.3	0.35326	5.76655	192.4	0.37765	6.16469
97.2	0.33936	5.53965	145.3	0.35395	5.77781	193.4	0.37787	6.16828
98.2	0.34010	5.55173	146.3	0.35433	5.78402	194.4	0.37799	6.17024
99.2	0.34049	5.55809	147.3	0.35469	5.78989	195.4	0.37817	6.17318
100.2	0.34088	5.56446	148.3	0.35527	5.79936	196.4	0.37838	6.17660
101.2	0.34131	5.57148	149.3	0.35562	5.80507	197.4	0.37927	6.19113
102.2	0.34179	5.57932	150.3	0.35599	5.81111	198.4	0.38035	6.20876
103.2	0.34210	5.58438	151.3	0.35705	5.82842	199.4	0.38105	6.22019
104.2	0.34217	5.58552	152.3	0.35793	5.84278	200.4	0.38183	6.23292
105.2	0.34237	5.58878	153.3	0.35854	5.85274	201.4	0.38293	6.25088
106.3	0.34262	5.59286	154.3	0.35903	5.86074	202.4	0.38393	6.26720
107.3	0.34325	5.60315	155.3	0.35897	5.85976	203.4	0.38508	6.28597
108.3	0.34355	5.60805	156.3	0.35897	5.85976	204.4	0.38649	6.30899
109.3	0.34400	5.61539	157.3	0.35906	5.86123	205.4	0.38835	6.33935
110.3	0.34447	5.62306	158.3	0.35915	5.86270	206.4	0.39011	6.36808
111.3	0.34465	5.62600	159.3	0.35920	5.86351	207.4	0.39190	6.39730
112.3	0.34487	5.62959	160.3	0.35934	5.86580	208.4	0.39330	6.42015
113.3	0.34519	5.63482	161.3	0.36017	5.87935	209.4	0.39462	6.44170
114.3	0.34528	5.63629	162.3	0.36075	5.88881	210.4	0.39524	6.45182
115.3	0.34543	5.63873	163.3	0.36109	5.89436	211.4	0.39518	6.45084
116.3	0.34578	5.64445	164.3	0.36164	5.90334	212.4	0.39496	6.44725
117.3	0.34634	5.65359	165.3	0.36170	5.90432	213.4	0.39573	6.45982
118.3	0.34663	5.65832	166.3	0.36143	5.89991	214.4	0.39745	6.48790
119.3	0.34720	5.66763	167.3	0.36133	5.89828	215.4	0.40014	6.53181
120.3	0.34747	5.67203	168.3	0.36151	5.90122	216.4	0.40375	6.59074
121.3	0.34790	5.67905	169.4	0.36208	5.91053	217.4	0.40852	6.66860
122.3	0.34839	5.68705	170.4	0.36359	5.93517	218.4	0.41320	6.74500
123.3	0.34892	5.69570	171.4	0.36521	5.96162	219.4	0.41849	6.83135
124.3	0.34922	5.70060	172.4	0.36634	5.98006	220.4	0.42490	6.93599
125.3	0.34937	5.70305	173.4	0.36719	5.99394	221.4	0.43219	7.05499
126.3	0.34972	5.70876	174.4	0.36708	5.99214	222.4	0.44012	7.18444
127.3	0.34995	5.71252	175.4	0.36704	5.99149	223.4	0.44951	7.33772
128.3	0.35015	5.71578	176.4	0.36709	5.99231	224.4	0.46116	7.52789
129.3	0.35056	5.72247	177.4	0.36662	5.98464	225.4	0.48626	7.93762
130.3	0.35081	5.72656	178.4	0.36679	5.98741	226.4	0.76613	12.50616
131.3	0.35121	5.73309	179.4	0.36674	5.98659	227.4	1.08586	17.72537
132.3	0.35150	5.73782	180.4	0.36752	5.99933	228.4	0.65497	10.69161
133.3	0.35147	5.73733	181.4	0.36818	6.01010	229.4	0.47818	7.80572
134.3	0.35151	5.73798	182.4	0.36866	6.01794	230.4	0.41313	6.74386
135.3	0.35155	5.73864	183.4	0.36932	6.02871	231.5	0.38680	6.31405
136.3	0.35186	5.74370	184.4	0.36990	6.03818	232.5	0.37498	6.12110
137.3	0.35220	5.74925	185.4	0.37033	6.04520	233.5	0.36924	6.02740
138.3	0.35253	5.75463	186.4	0.37105	6.05695	234.5	0.36558	5.96766
139.3	0.35253	5.75463	187.4	0.37206	6.07344	235.5	0.36287	5.92342
140.3	0.35239	5.75235	188.4	0.37313	6.09090	236.5	0.36119	5.89600
141.3	0.35254	5.75480	189.4	0.37400	6.10511	237.5	0.35926	5.86449

Table IV. (A) Heat Capacity for PZT95/5(1.8Nb) Ceramic (continued).

Temp. (°C)	Cp (J/g*K)	Cp cal/(g-mole*K)	Temp. (°C)	Cp (J/g*K)	Cp cal/(g-mole*K)
238.5	0.35800	5.84392	286.5	0.34642	5.65489
239.5	0.35687	5.82548	287.5	0.34675	5.66028
240.5	0.35632	5.81650	288.5	0.34707	5.66550
241.5	0.35585	5.80883	289.5	0.34717	5.66714
242.5	0.35559	5.80458	290.5	0.34717	5.66714
243.5	0.35516	5.79756	291.5	0.34712	5.66632
244.5	0.35482	5.79201	292.5	0.34701	5.66453
245.5	0.35441	5.78532	293.5	0.34712	5.66632
246.5	0.35384	5.77602	294.6	0.34700	5.66436
247.5	0.35286	5.76002	295.6	0.34731	5.66942
248.5	0.35233	5.75137	296.6	0.34728	5.66893
249.5	0.35171	5.74125	297.6	0.34680	5.66110
250.5	0.35109	5.73113	298.6	0.34622	5.65163
251.5	0.35089	5.72786	299.6	0.34626	5.65228
252.5	0.35033	5.71872			
253.5	0.34981	5.71023			
254.5	0.34975	5.70925			
255.5	0.34938	5.70321			
256.5	0.34882	5.69407			
257.5	0.34901	5.69717			
258.5	0.34863	5.69097			
259.5	0.34903	5.69750			
260.5	0.34915	5.69946			
261.5	0.34924	5.70093			
262.5	0.34899	5.69685			
263.5	0.34828	5.68526			
264.5	0.34852	5.68917			
265.5	0.34852	5.68917			
266.5	0.34803	5.68118			
267.5	0.34781	5.67758			
268.5	0.34705	5.66518			
269.5	0.34691	5.66289			
270.5	0.34670	5.65947			
271.5	0.34667	5.65898			
272.5	0.34636	5.65391			
273.5	0.34640	5.65457			
274.5	0.34691	5.66289			
275.5	0.34704	5.66502			
276.5	0.34744	5.67154			
277.5	0.34779	5.67726			
278.5	0.34771	5.67595			
279.5	0.34763	5.67465			
280.5	0.34747	5.67203			
281.5	0.34689	5.66257			
282.5	0.34655	5.65702			
283.5	0.34622	5.65163			
284.5	0.34605	5.64885			

Table IV. (B) Heat Capacity of PSZT Ceramic

Temp. (°C)	Cp (J/(g*K)	Cp (cal/(g-mole*K)	Temp. (°C)	Cp (J/(g*K)	Cp (cal/(g-mole*K)	Temp. (°C)	Cp (J/(g*K)	Cp (cal/(g-mole*K)
-50.0	0.28807	4.74281	-1.9	0.30940	5.09398	46.2	0.32784	5.39758
-49.0	0.28854	4.75054	-0.9	0.30964	5.09794	47.2	0.32819	5.40334
-48.0	0.28913	4.76026	0.1	0.31028	5.10847	48.2	0.32883	5.41388
-47.0	0.28995	4.77376	1.1	0.31086	5.11802	49.2	0.32930	5.42162
-46.0	0.28991	4.77310	2.1	0.31111	5.12214	50.2	0.32976	5.42919
-45.0	0.29026	4.77886	3.1	0.31170	5.13185	51.2	0.33020	5.43644
-44.0	0.29045	4.78199	4.1	0.31213	5.13893	52.2	0.33084	5.44697
-43.0	0.29040	4.78117	5.1	0.31263	5.14716	53.2	0.33118	5.45257
-42.0	0.29112	4.79302	6.1	0.31340	5.15984	54.2	0.33150	5.45784
-41.0	0.29077	4.78726	7.1	0.31365	5.16396	55.2	0.33206	5.46706
-40.0	0.29146	4.79862	8.1	0.31467	5.18075	56.2	0.33246	5.47365
-39.0	0.29129	4.79582	9.1	0.31542	5.19310	57.2	0.33280	5.47924
-38.0	0.29170	4.80257	10.1	0.31623	5.20643	58.2	0.33296	5.48188
-37.0	0.29151	4.79944	11.1	0.31691	5.21763	59.2	0.33355	5.49159
-36.0	0.29164	4.80158	12.1	0.31730	5.22405	60.2	0.33366	5.49340
-35.0	0.29194	4.80652	13.1	0.31746	5.22668	61.2	0.33399	5.49884
-34.0	0.29071	4.78627	14.1	0.31737	5.22520	62.2	0.33406	5.49999
-33.0	0.29038	4.78084	15.1	0.31774	5.23129	63.2	0.33444	5.50624
-32.0	0.29018	4.77754	16.1	0.31836	5.24150	64.2	0.33451	5.50740
-31.0	0.29067	4.78561	17.1	0.31930	5.25698	65.2	0.33494	5.51448
-30.0	0.29146	4.79862	18.1	0.31962	5.26225	66.2	0.33492	5.51415
-29.0	0.29269	4.81887	19.1	0.32036	5.27443	67.2	0.33522	5.51909
-28.0	0.29395	4.83961	20.1	0.32063	5.27888	68.2	0.33541	5.52221
-27.0	0.29570	4.86843	21.1	0.32092	5.28365	69.2	0.33573	5.52748
-26.0	0.29945	4.93017	22.1	0.32095	5.28414	70.2	0.33650	5.54016
-25.0	0.30614	5.04031	23.1	0.32091	5.28349	71.2	0.33728	5.55300
-24.0	0.30474	5.01726	24.1	0.32134	5.29056	72.2	0.33803	5.56535
-23.0	0.30516	5.02418	25.1	0.32150	5.29320	73.2	0.33878	5.57770
-22.0	0.30513	5.02368	26.1	0.32157	5.29435	74.2	0.33952	5.58988
-21.0	0.30199	4.97198	27.1	0.32211	5.30324	75.2	0.34046	5.60536
-20.0	0.30309	4.99010	28.1	0.32226	5.30571	76.2	0.34107	5.61540
-19.0	0.30336	4.99454	29.1	0.32271	5.31312	77.2	0.34186	5.62841
-17.9	0.30279	4.98516	30.1	0.32290	5.31625	78.2	0.34213	5.63285
-16.9	0.30417	5.00788	31.1	0.32361	5.32794	79.2	0.34273	5.64273
-15.9	0.30557	5.03093	32.1	0.32411	5.33617	80.2	0.34307	5.64833
-14.9	0.30582	5.03504	33.1	0.32467	5.34539	81.2	0.34327	5.65162
-13.9	0.30688	5.05249	34.1	0.32524	5.35477	82.2	0.34400	5.66364
-12.9	0.30722	5.05809	35.1	0.32206	5.30242	83.2	0.34491	5.67862
-11.9	0.30788	5.06896	36.1	0.32600	5.36729	84.2	0.34587	5.69443
-10.9	0.30806	5.07192	37.1	0.32613	5.36943	85.2	0.34742	5.71995
-9.9	0.30841	5.07768	38.1	0.32645	5.37470	86.2	0.34982	5.75946
-8.9	0.30857	5.08032	39.1	0.32672	5.37914	87.2	0.35332	5.81709
-7.9	0.30785	5.06846	40.1	0.32714	5.38606	88.2	0.35835	5.89990
-6.9	0.30871	5.08262	41.1	0.32708	5.38507	89.2	0.36679	6.03886
-5.9	0.30867	5.08196	42.1	0.32715	5.38622	90.2	0.37873	6.23544
-4.9	0.30845	5.07834	43.1	0.32726	5.38803	91.2	0.39285	6.46791
-3.9	0.30870	5.08246	44.2	0.32747	5.39149	92.2	0.40200	6.61856
-2.9	0.30885	5.08493	45.2	0.32741	5.39050	93.2	0.40001	6.58579

Table IV (B) Heat Capacity of PSZT Ceramic (continued).

Temp. (°C)	Cp (J/(g*K)	Cp (cal/(g-mole*K)	Temp. (°C)	Cp (J/(g*K)	Cp (cal/(g-mole*K)	Temp. (°C)	Cp (J/(g*K)	Cp (cal/(g-mole*K)
94.2	0.38992	6.41967	142.3	0.35724	5.88162	190.4	0.40075	6.59798
95.2	0.37827	6.22786	143.3	0.35777	5.89035	191.4	0.37768	6.21815
96.2	0.36830	6.06372	144.3	0.35825	5.89825	192.4	0.36796	6.05812
97.2	0.36111	5.94534	145.3	0.35917	5.91340	193.4	0.36319	5.97959
98.2	0.35613	5.86335	146.3	0.35961	5.92064	194.4	0.36030	5.93200
99.2	0.35248	5.80326	147.3	0.36075	5.93941	195.4	0.35833	5.89957
100.2	0.35012	5.76440	148.3	0.36129	5.94830	196.4	0.35649	5.86928
101.2	0.34842	5.73641	149.3	0.36223	5.96378	197.4	0.35589	5.85940
102.2	0.34723	5.71682	150.3	0.36287	5.97432	198.4	0.35503	5.84524
103.2	0.34640	5.70315	151.3	0.36416	5.99556	199.4	0.35521	5.84820
104.2	0.34549	5.68817	152.3	0.36537	6.01548	200.4	0.35506	5.84573
105.2	0.34523	5.68389	153.3	0.36607	6.02700	201.4	0.35500	5.84475
106.3	0.34495	5.67928	154.3	0.36718	6.04528	202.4	0.35419	5.83141
107.3	0.34481	5.67698	155.3	0.36751	6.05071	203.4	0.35305	5.81264
108.3	0.34478	5.67648	156.3	0.36794	6.05779	204.4	0.35260	5.80523
109.3	0.34481	5.67698	157.3	0.36814	6.06108	205.4	0.35226	5.79963
110.3	0.34492	5.67879	158.3	0.36847	6.06652	206.4	0.35162	5.78910
111.3	0.34541	5.68685	159.3	0.3691	6.07689	207.4	0.35058	5.77197
112.3	0.34585	5.69410	160.3	0.36998	6.09138	208.4	0.34941	5.75271
113.3	0.34629	5.70134	161.3	0.3709	6.10652	209.4	0.34856	5.73872
114.3	0.34662	5.70678	162.3	0.37202	6.12496	210.4	0.34774	5.72522
115.3	0.34694	5.71204	163.3	0.37317	6.14390	211.4	0.34700	5.71303
116.3	0.34753	5.72176	164.3	0.37498	6.17370	212.4	0.34676	5.70908
117.3	0.34796	5.72884	165.3	0.37624	6.19444	213.4	0.34657	5.70595
118.3	0.34840	5.73608	166.3	0.37731	6.21206	214.4	0.34705	5.71386
119.3	0.34912	5.74794	167.3	0.3786	6.23330	215.4	0.34731	5.71814
120.3	0.34965	5.75666	168.3	0.37997	6.25585	216.4	0.34820	5.73279
121.3	0.35029	5.76720	169.4	0.38131	6.27792	217.4	0.34865	5.74020
122.3	0.35074	5.77461	170.4	0.38279	6.30228	218.4	0.34862	5.73970
123.3	0.35133	5.78432	171.4	0.38444	6.32945	219.4	0.34894	5.74497
124.3	0.35173	5.79091	172.4	0.3857	6.35019	220.4	0.34877	5.74217
125.3	0.35227	5.79980	173.4	0.38704	6.37225	221.4	0.34843	5.73658
126.3	0.35236	5.80128	174.4	0.3888	6.40123	222.4	0.34859	5.73921
127.3	0.35304	5.81248	175.4	0.39069	6.43235	223.4	0.34897	5.74547
128.3	0.35331	5.81692	176.4	0.39305	6.47120	224.4	0.34880	5.74267
129.3	0.35382	5.82532	177.4	0.39585	6.51730	225.4	0.34861	5.73954
130.3	0.35389	5.82647	178.4	0.39867	6.56373	226.4	0.34878	5.74234
131.3	0.35443	5.83536	179.4	0.40212	6.62053	227.4	0.34871	5.74119
132.3	0.35493	5.84359	180.4	0.40696	6.70022	228.4	0.34913	5.74810
133.3	0.35504	5.84540	181.4	0.41304	6.80032	229.4	0.34941	5.75271
134.3	0.35530	5.84968	182.4	0.42101	6.93154	230.4	0.35008	5.76374
135.3	0.35543	5.85182	183.4	0.43409	7.14689	231.5	0.35042	5.76934
136.3	0.35586	5.85890	184.4	0.45884	7.55437	232.5	0.35050	5.77066
137.3	0.35621	5.86467	185.4	0.52272	8.60610	233.5	0.35072	5.77428
138.3	0.35643	5.86829	186.4	0.71566	11.78268	234.5	0.35061	5.77247
139.3	0.35669	5.87257	187.4	0.93508	15.39522	235.5	0.35004	5.76308
140.3	0.35678	5.87405	188.4	0.62671	10.31820	236.5	0.34990	5.76078
141.3	0.35704	5.87833	189.4	0.46118	7.59290	237.5	0.34946	5.75353

Table IV. (B) Heat Capacity for PSZT Ceramic (continued).

Temp. (°C)	Cp (J/(g*K)	Cp (cal/(g-mole*K)	Temp. (°C)	Cp (J/(g*K)	Cp (cal/(g-mole*K)
238.5	0.34949	5.75403	286.5	0.34539	5.68653
239.5	0.34918	5.74892	287.5	0.34531	5.68521
240.5	0.34921	5.74942	288.5	0.34466	5.67451
241.5	0.34896	5.74530	289.5	0.34471	5.67533
242.5	0.34893	5.74481	290.5	0.34456	5.67286
243.5	0.34891	5.74448	291.5	0.34441	5.67039
244.5	0.34920	5.74925	292.5	0.34457	5.67303
245.5	0.34855	5.73855	293.5	0.34517	5.68290
246.5	0.34824	5.73345	294.6	0.34529	5.68488
247.5	0.34767	5.72406	295.6	0.34566	5.69097
248.5	0.34695	5.71221	296.6	0.34613	5.69871
249.5	0.34635	5.70233	297.6	0.34638	5.70283
250.5	0.34549	5.68817	298.6	0.34646	5.70414
251.5	0.34549	5.68817	299.6	0.34662	5.70678
252.5	0.34539	5.68653			
253.5	0.34551	5.68850			
254.5	0.34591	5.69509			
255.5	0.34552	5.68867			
256.5	0.34489	5.67829			
257.5	0.34419	5.66677			
258.5	0.34353	5.65590			
259.5	0.34334	5.65277			
260.5	0.34363	5.65755			
261.5	0.34439	5.67006			
262.5	0.34511	5.68192			
263.5	0.34580	5.69328			
264.5	0.34655	5.70562			
265.5	0.34705	5.71386			
266.5	0.34727	5.71748			
267.5	0.34728	5.71764			
268.5	0.34703	5.71353			
269.5	0.34613	5.69871			
270.5	0.34498	5.67978			
271.5	0.34442	5.67056			
272.5	0.34349	5.65524			
273.5	0.34342	5.65409			
274.5	0.34402	5.66397			
275.5	0.34442	5.67056			
276.5	0.34493	5.67895			
277.5	0.34595	5.69575			
278.5	0.34661	5.70661			
279.5	0.34700	5.71303			
280.5	0.34662	5.70678			
281.5	0.34599	5.69640			
282.5	0.34577	5.69278			
283.5	0.34553	5.68883			
284.5	0.34578	5.69295			
285.5	0.34588	5.69459			

Table V. (A) The Constant-Pressure Heat Capacity for Different Phases in PZT95/5(1.8Nb) ceramic. (Cp = a + b*T; Units: Cp: J/(g*K); T: K)

Phase	Temperature range (°C)	a	b	R^2
FE_{RL}	-10 to 42	0.2073	0.0004	0.9551
FE_{RH}	66 to 192	0.2195	0.0003	0.9863
PE	256 to 300	0.3754	-0.00005	0.5137

Table V. (B) The Constant-Pressure Heat Capacity for Different Phases in PSZT Ceramic. (Cp = a + b*T; Units: Cp: J/(g*K); T: K)

Phase	Temperature range (°C)	a	b	R^2
FE_{RL}	-20 to 82	0.2081	0.0004	0.9929
FE_{RH}	108 to 175	0.1695	0.0005	0.9727
PE	198 to 300	0.3847	-0.00007	0.5853

Table VI. (A) Enthalpy Change Associated with Phase Transformation in PZT95/5(1.8Nb) Ceramic.

Phase transformation	Enthalpy (J/g)	Enthalpy (cal/mole)
FE_{RL}-to-FE_{RH}	0.5322	43.4377
FE_{RH}-to-PE	2.096	171.0735

Table VI. (B) Enthalpy Change Associated with Phase Transformation in PSZT Ceramic.

Phase transformation	Enthalpy (J/g)	Enthalpy (cal/mole)
FE_{RL}-to-FE_{RH}	0.5091	41.9098
FE_{RH}-to-PE	2.1195	174.4803

Table VII. (A) Thermal Diffusivity and Thermal Conductivity for PZT95/5(1.8Nb) Ceramic at Different Temperatures.

PZT95/5(1.8Nb)				
Temperature (°C)	Thermal diffusivity (cm^2/s)	Heat capacity (J/(K*g))	Density (g/cm^3)	Thermal conductivity (W/(K*cm))
-59	0.005833	0.28530	7.377	0.012276
-33	0.005591	0.29300	7.374	0.012079
-13	0.005395	0.30776	7.371	0.012239
-1	0.005283	0.31670	7.369	0.012330
1	0.005272	0.31434	7.369	0.012211
22	0.005053	0.32242	7.366	0.012001
41	0.004896	0.33106	7.366	0.011940
48	0.004307	0.37983	7.364	0.012047
50	0.004754	0.41634	7.329	0.014507
74	0.004705	0.33534	7.328	0.011561
87	0.004670	0.33575	7.328	0.011489
89	0.004665	0.33646	7.328	0.011501
98	0.004636	0.34010	7.328	0.011555

Table VII. (B) Thermal Diffusivity and Thermal Conductivity for PSZT Ceramic at Different Temperatures.

PSZT				
Temperature (°C)	Thermal diffusivity (cm^2/s)	Heat capacity (J/(K*g))	Density (g/cm^3)	Thermal conductivity (W/(K*cm))
-59	0.005820	0.28140	7.729	0.012658
-13	0.005437	0.30614	7.723	0.012856
-10	0.005404	0.30806	7.723	0.012858
0	0.005319	0.30940	7.722	0.012709
22	0.005169	0.32150	7.719	0.012827
41	0.005060	0.32715	7.717	0.012775
48	0.005020	0.32883	7.717	0.012739
50	0.005009	0.32976	7.716	0.012747
74	0.004828	0.33952	7.714	0.012645
87	0.004786	0.37873	7.713	0.013979
89	0.004788	0.36679	7.687	0.013499
98	0.004734	0.35613	7.687	0.012958

Table VIII. Calculated Phonon Mean Free Path in PZT95/5(1.8Nb) and PSZT Ceramics at Room Temperature (FE_{RL}; R3c).

Material	Thermal diffusivity (α_d, cm^2/sec)	Average elastic wave velocity (v, m/sec)	Mean free path (Å) $l = 3\ \alpha_d/v$
PZT95/5(1.8Nb)	0.005053	4332.9	3.58
PSZT	0.005171	4360.0	3.56

Table IX. Average Thermal Conductivity for PZT95/5(1.8Nb) and PSZT Ceramics.

Material	Temperature range	Phase	Thermal conductivity (W/(K*cm))
PZT95/5(1.8Nb)	-70°C – 48°C	FE_{RL}	0.01214±0.00014
	60°C – 100°C	FE_{RH}	0.01153±0.00004
PSZT	-70°C – 80°C	FE_{RL}	0.01276±0.00008

Table X. Calculated Grüneisen Constant for PZT95/5(1.8Nb) and PSZT Ceramics.

Material	Volumetric thermal expansion (1/K)	Volume per mass (m^3/Kg)	Heat capacity C_v (~ C_p) (J/(Kg*K)	Isothermal compressibility (m^2/N)	Grüneisen constant
PZT95/5 (1.8Nb) @ 25°C (FE_{RL})	1.994×10^{-5} (based on as-sintered sample)	1.358×10^{-4}	3.249×10^{2}	1.457×10^{-11}	0.572
PSZT @ 25°C (FE_{RL})	1.942×10^{-5} (based on as-sintered sample)	1.296×10^{-4}	3.215×10^{2}	1.285×10^{-11}	0.611
PSZT @ 98°C (FE_{RH})	2.550×10^{-6} (based on as-sintered sample)	1.301×10^{-4}	3.513×10^{2}	1.156×10^{-11}	0.082

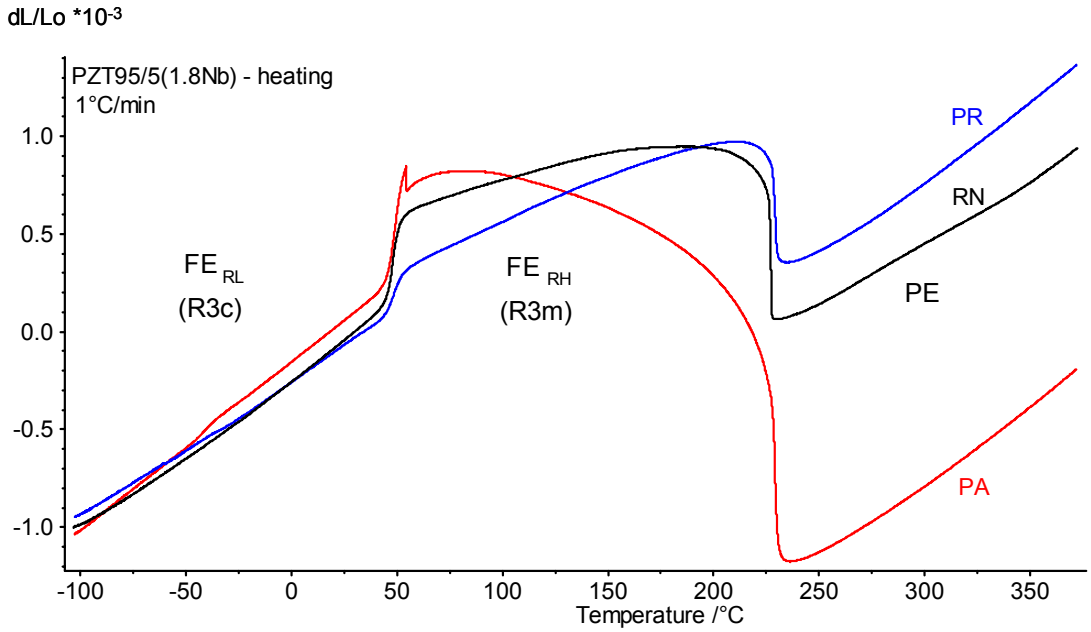

Figure 1. Thermal expansion behavior of PZT95/5(1.8Nb) ceramics during a heating cycle. Thermal strains are reported for as-sintered sample (RN; black), as well as for parallel (PA; red) and perpendicular (PR; blue) to the spontaneous polarization direction $[111]_c$.

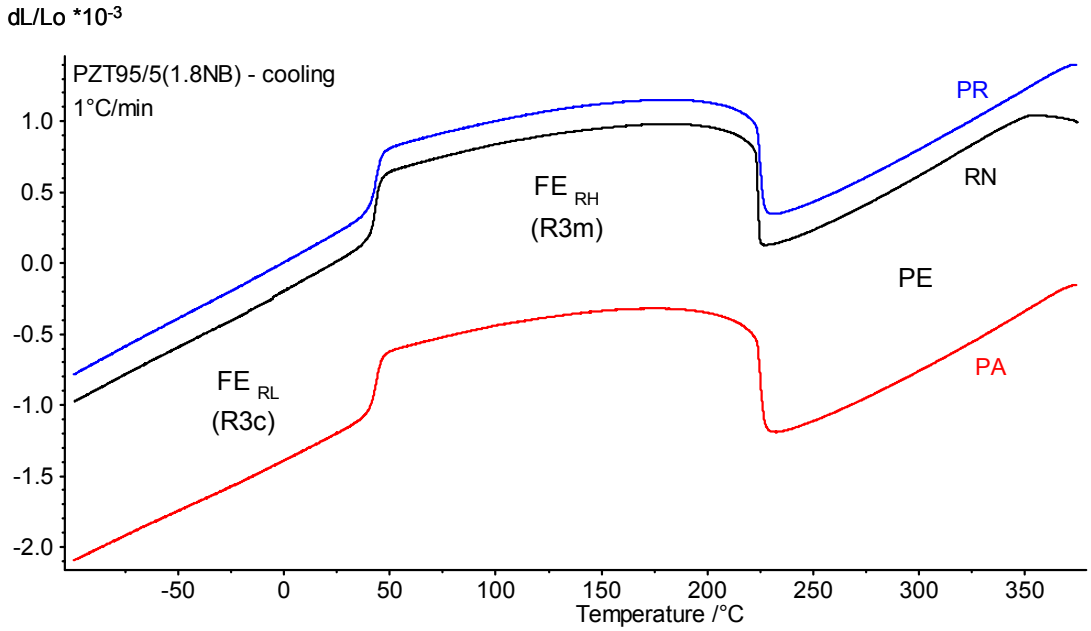

Figure 2. Thermal expansion behavior of PZT95/5(1.8Nb) ceramics during a cooling cycle. Thermal strains are reported for as-sintered sample (RN; black), as well as for parallel (PA; red) and perpendicular (PR; blue) to the spontaneous polarization direction $[111]_c$.

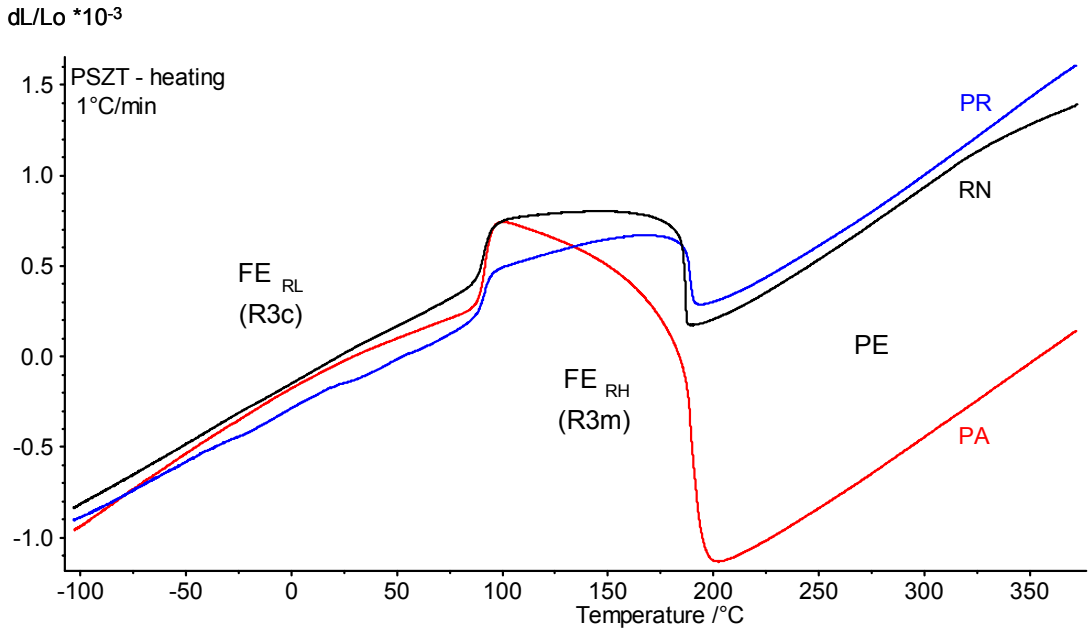

Figure 3. Thermal expansion behavior of PSZT ceramics during a heating cycle. Thermal strains are reported for as-sintered sample (RN; black), as well as for parallel (PA; red) and perpendicular (PR; blue) to the spontaneous polarization direction $[111]_c$.

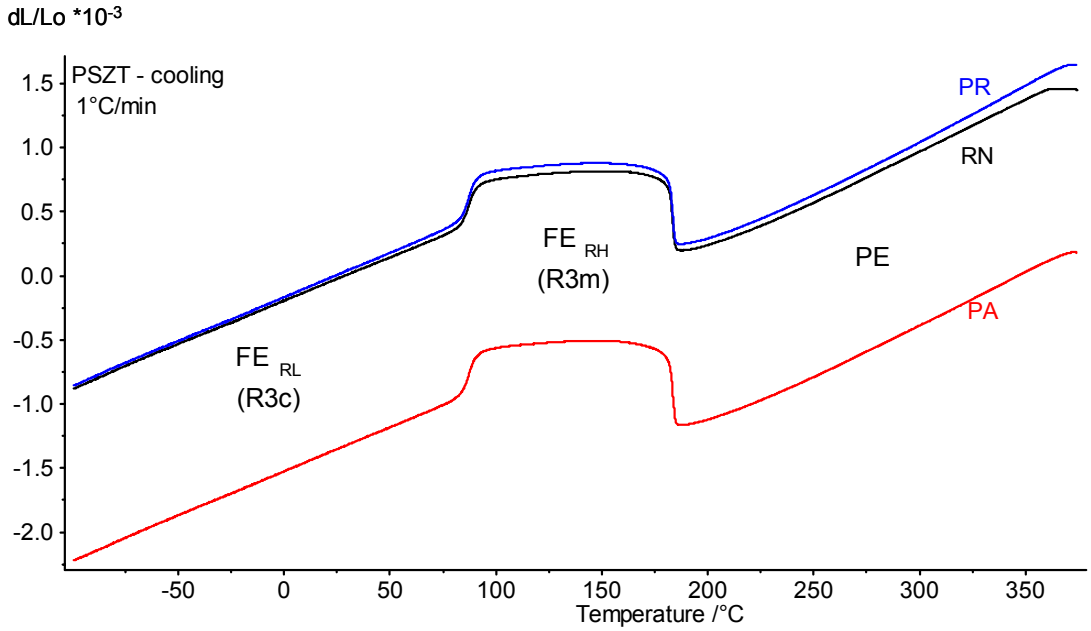

Figure 4. Thermal expansion behavior of PSZT95/5 ceramics during a cooling cycle. Thermal strains are reported for as-sintered sample (RN; black), as well as for parallel (PA; red) and perpendicular (PR; blue) to the spontaneous polarization direction $[111]_c$.

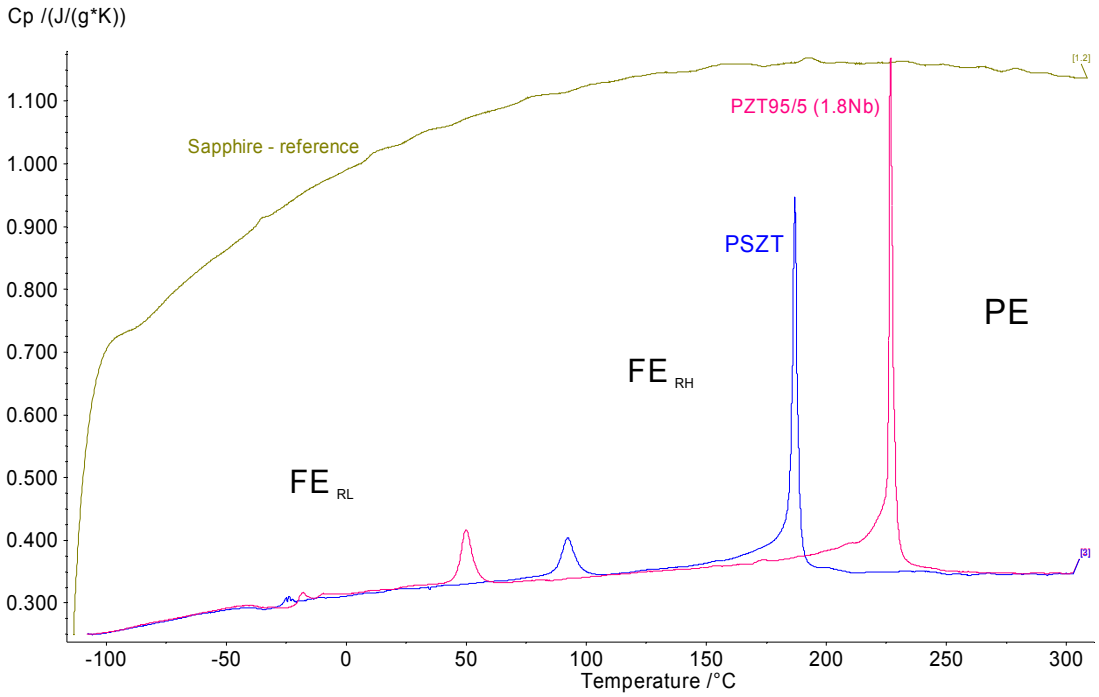

Figure 5. The constant pressure heat capacity of PZT95/5(1.8Nb) and PSZT ceramics at different temperatures. The heat capacity of sapphire is used as a reference material for heat capacity calculation.

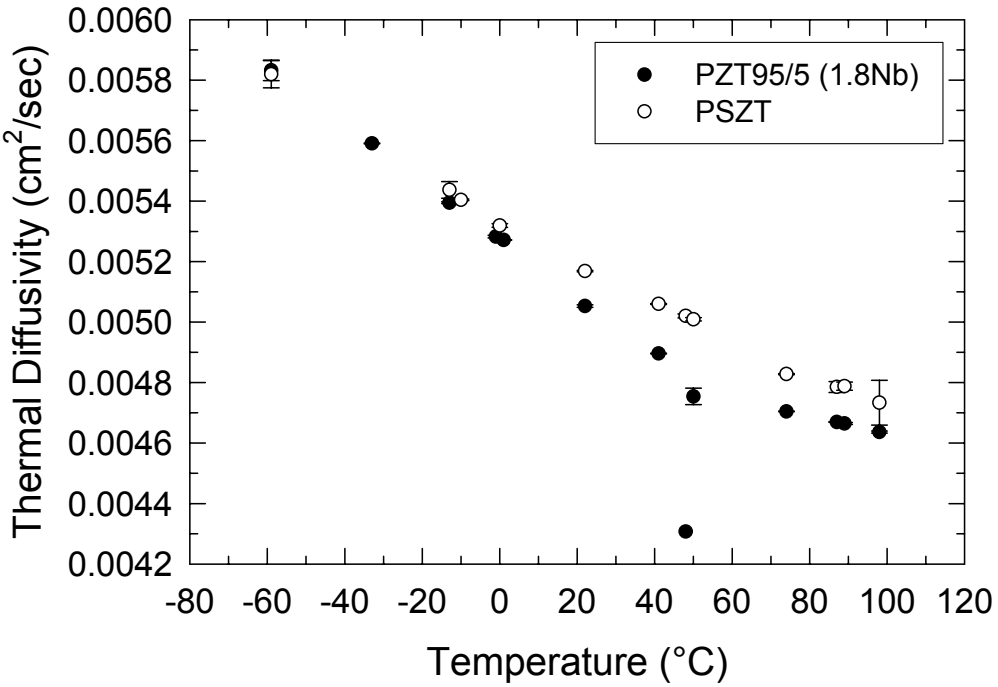

Figure 6. Thermal diffusivity of PZT95/5(1.8Nb) and PSZT ceramics from -60°C to 100°C. Three measurements were made at each temperature.

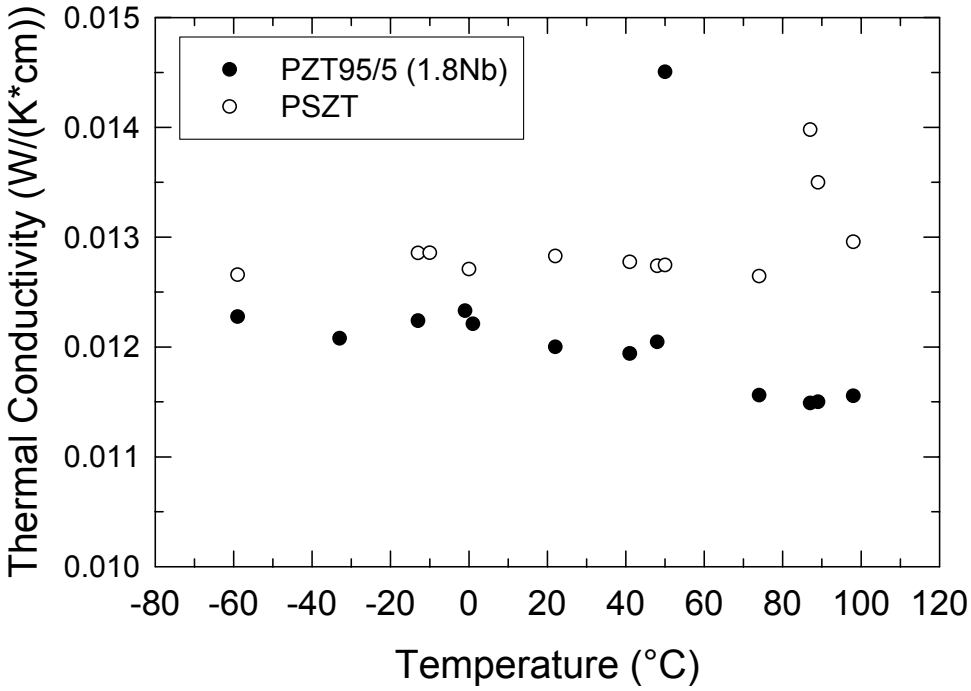

Figure 7. Calculated thermal conductivity of PZT95/5(1.8Nb) and PSZT ceramics.

Distribution:

1	MS1245	Christopher B. DiAntonio, 02454
1	MS1245	Timothy J. Gardner, 02454
1	MS1245	David M. Goy, 02454
1	MS1245	Steve J. Lockwood, 02454
1	MS1245	Roger H. Moore, 02454
1	MS0959	Ronnie G. Stone, 02454
1	MS1245	Chad S. Watson, 02454
3	MS1245	Pin Yang, 02454
1	MS0889	S. Jill Glass, 01825
1	MS0889	Rajan Tandon, 01825
1	MS1411	James A. Voigt, 01816
1	MS1411	Bruce A. Tuttle, 01816
1	MS1421	George A. Samara, 01130
1	MS0555	Steven J. Younghouse, 01522
1	MS1159	Scott C. Jones, 01344
1	MS0557	Todd W. Simmermacher, 01523
1	MS0335	Stephen T. Montgomery, 02725
1	MS0335	Timothy W. Scofield, 02725
1	MS0515	Todd A. Haverlock, 02723
1	MS0515	Alexander W. Roesler, 02723
1	MS0515	Luis A. Paz, 02723
1	MS0515	Robert J. Stiers, 02723
1	MS0515	Karen Shin, 02722
1	MS0634	Jeffrey D. Keck, 02951
2	MS9960	Central Technical Files, 08944
2	MS0899	Technical Library, 4536